Title
Progress in metal-supported solid oxide electrolysis cells: A review

Journal
International Journal of Hydrogen Energy, 45(46)

ISSN
0360-3199

Author
Tucker, Michael C

Publication Date
2020-09-01

DOI
10.1016/j.ijhydene.2020.06.300

Peer reviewed

Progress in Metal-Supported Solid Oxide Electrolysis Cells: A Review

Michael C. Tucker*

Energy Conversion Group, Energy Technologies Area

Lawrence Berkeley National Laboratory

1 Cyclotron Rd

Berkeley, CA 94720 USA

Abstract

There is increasing global interest in using solid oxide electrochemical cells to perform electrolysis. Metal-supported solid oxide electrolysis cells (MS-SOEC) are being developed with stainless steel and Ni-based supports. The use of porous metal to support the electrochemically-active layers is anticipated to improve mechanical strength, decrease cost, and increase tolerance to aggressive operating conditions, including rapid thermal excursions. This review summarizes and analyzes the previous decade of progress in MS-SOEC development, and identifies critical needs for future work.

Metal-supported; SOEC; high temperature electrolysis

*mctucker@lbl.gov

Phone 1-510-486-5304

Fax 1-510-486-4260

LBNL; 1 Cyclotron Rd; MS 62-203; Berkeley CA 94720; USA

1. The opportunity for high-temperature metal-supported electrolysis cells

Electrolysis cells utilize a direct electrochemical current to drive a non-spontaneous reaction, such as splitting of water to produce oxygen and hydrogen. High temperature solid oxide electrolysis cells typically operate in the range 500 to 900°C, and utilize ceramic oxide electrolyte layers that primarily conduct either oxide ions or protons. Operation at such high temperature provides distinct benefits over commercially-available proton exchange membrane (PEM) and alkaline exchange membrane (AEM) electrolyzers that operate between room temperature and ~100°C. In particular, inexpensive non-platinum group materials can be used as catalysts, the ceramic membrane is impermeable so high purity products are easily obtained, and electrical energy and total energy demand is lower due to the enthalpy difference between liquid water and steam and in-situ consumption of resistive heat from the cell and external sources [1]. High-temperature oxide-conducting cells are commonly referred to as solid oxide electrolysis cells (SOEC), and proton-conducting cells are termed proton-conducting electrolysis cells (PCEC) although most proton-conducting materials are also oxide ceramics. By far, the most commonly studied application for both types is steam electrolysis to produce hydrogen. This is due to the similarity to standard solid oxide fuel cells utilizing hydrogen fuel [2], and the promise of utilizing hydrogen as an energy carrier throughout the economy [3]. A number of other electrolysis applications have been demonstrated with SOEC, including: ethylene production from methane [4]; co-electrolysis of carbon dioxide and steam to produce syngas or methane [5, 6]; methane-assisted steam electrolysis to produce hydrogen with low electrical energy requirement [7]; and, carbon dioxide reduction to produce CO for further chemical reactions [8], or to generate oxygen from the Mars atmosphere for life support [9]. Electrolysis is also a natural step in operation of reversible solid oxide cells (rSOC), which switch between fuel cell and electrolysis modes to store energy, typically as compressed hydrogen [10, 11]. Several recent reviews on the topic of high temperature electrolysis are available [1, 2, 12].

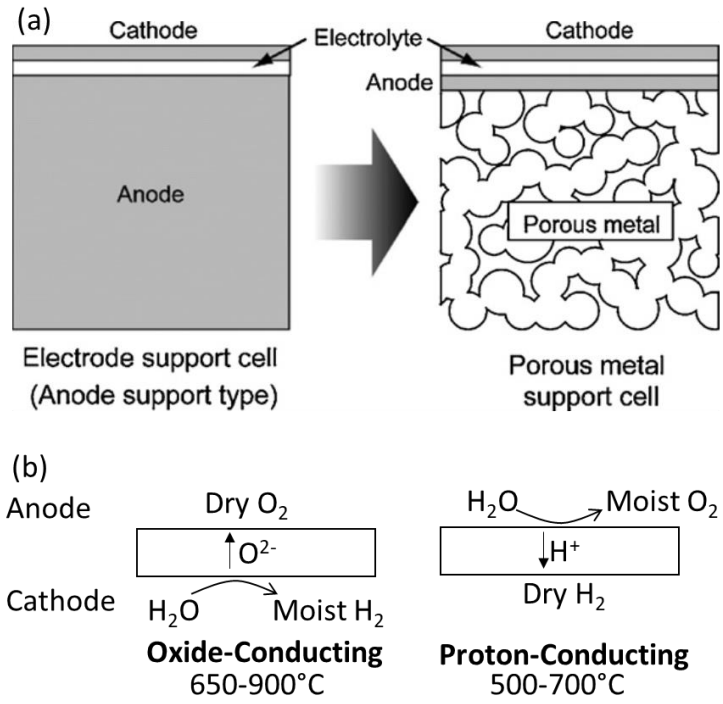

Figure 1. Metal-supported cell structure and operating environment for steam electrolysis. (a) The concept of the MS-SOEC is to replace the Ni-YSZ electrode support with a porous stainless steel or other metal. Reproduced with permission from Reference [17]. (b) Conditions for SOEC steam electrolysis operation are quite different for cells based on oxide-conducting and proton-conducting electrolytes. Note that air is frequently use to represent the anode atmosphere for oxide-conducting SOECs.

This review will focus specifically on metal-supported solid oxide electrolysis cells and the subset metal-supported proton conducting electrolysis cells (MS-PCEC), collectively referred to in this article as MS-SOEC, and sometimes referred to as MSC in other publications. The fabrication, materials, and structure of MS-SOECs are analogous to metal-supported solid oxide fuel cells (MS-SOFC), which have achieved a high level of commercial demonstration by companies including Ceres Power and Topsoe Fuel Cells, and for which several reviews are available [13-16]. The fundamental concept of the MS-SOC is to support thin

ceramic electrode/electrolyte layers on low-cost, robust stainless steel metal layers, Fig 1 [17]. The expensive ceramic electrochemical active layers are only as thick as necessary for electrochemical function, minimizing cell material cost and maximizing cell strength. This eliminates the issue of brittle failure associated with conventional SOFCs. This issue is also largely mitigated by the use of microtubular cells [18]. Whereas conventional SOFCs are typically heated to operating temperature over a few hours to minimize temperature gradients and thermal shock, MS-SOFCs can tolerate very large temperature gradients (>100°C/cm) and extremely rapid thermal cycling. Startup within 10 sec for a bare cell, and hundreds of 15 min startup cycles for cells mounted on testing hardware have been demonstrated [19, 20]; this is over an order of magnitude faster than conventional SOFCs can tolerate. Allowing the operating temperature to fluctuate in real time in response to variable load requirements is also enabled by MS-SOFCs [21]. Redox tolerance of MS-SOFCs is also exceptional. Redox cycling occurs when the anode side of the cell, typically containing Ni catalyst, is exposed to oxidizing conditions due to interruption of the fuel supply, leakage of air, or high fuel utilization leading to high steam content. This is easily catastrophic for conventional anode-supported SOFCs (ASC) because volume expansion of the anode as Ni converts to NiO cracks the electrolyte. In contrast, MS-SOFCs have a very strong metal support that constrains volume expansion, and in the case of catalysts introduced by infiltration, Ni is not part of the structural scaffold of the cell. MS-SOFCs readily survive complete oxidation and re-reduction of the anode, with little or no change in performance [19]. MS-SOFCs are also mechanically strong and flexible [22, 23]. In summary, MS-SOFCs are mechanically rugged, enable extremely fast start-up times and high redox tolerance, and are composed primarily of very low cost stainless steel as the metal support.

These same advantages are expected for MS-SOECs and enable several challenging electrolysis applications. For example, utilizing variable resources such as wind and solar to provide low-cost and renewable electricity to drive electrolysis is desirable, but inherently leads to transient operation of the

electrolysis device. Large changes in current or voltage can be tolerated by conventional SOECs [24], but rapid thermal transients are expected to be damaging. Temperature excursions can occur as instantaneous or daily variation in the electrical input and cause the SOEC to operate away from the thermo-neutral point in endothermic or exothermic regimes. The use of rSOC stacks to store renewable energy also causes large temperature excursions as the system switches between fuel cell and electrolysis modes [25, 26]. Co-electrolysis of steam and carbon dioxide is an endothermic reaction, and may create temperature gradients within an operating stack due to variation in current density and H_2O/CO_2 ratio when operated below the thermoneutral voltage [27]. The ability of MS-SOECs to tolerate temperature cycling and thermal gradients may be a key advantage for these applications. SOEC systems for space applications, such as electrolysis of CO_2 on Mars, will experience extreme forces and vibration during launch and re-entry [28]. The mechanical ruggedness of MS-SOECs may enable a thinner cell to tolerate this mechanical abuse, leading to a smaller and lighter stack, which is a critical advantage for aerospace applications.

Furthermore, the MS-SOEC architecture may solve some of the most problematic failure and degradation mechanisms observed for conventional SOECs. Delamination at the electrolyte/air electrode interface occurs at high current density due to excess oxygen pressure between the layers [29]. For the case of MS-SOECs and other SOEC configurations with electrodes formed by infiltrating catalysts into a porous scaffold of the electrolyte material [30-32], bonding at the electrolyte/electrode interface is greatly enhanced due to the continuous sintered ceramic electrolyte structure, and the dispersed catalyst will spread the reaction across a large area, reducing local current density. Both factors are expected to decrease the likelihood of delamination. The low catalyst processing temperature, small catalyst particle size, and electrode structure will also potentially mitigate microstructural evolution, and Ni migration and coarsening [33-35]. Formation of insulating species due to reaction between the Gd-doped ceria (CGO)

buffer layer and zirconia electrolyte [36] will also be eliminated, as this type of MS-SOEC does not have a buffer layer.

2. Cell fabrication and operation

Not surprisingly, most of the MS-SOEC results to date were reported by groups that have previously developed MS-SOFCs. In most cases, the existing MS-SOFC cell design is operated in electrolysis mode, and in a few cases catalyst composition is tailored for electrolysis operation. Development of oxide-conducting MS-SOECs is well under way, with various cell fabrication approaches providing functional cells and continuous operation for 1000 h or longer. Proton-conducting electrolyte materials are much more difficult to implement in MS-SOEC architectures, and although there has been progress on processing approaches, a viable cell is yet to be fabricated.

In electrolysis mode, oxidation occurs at the oxygen electrode so this is correctly called the anode, and the hydrogen electrode is the cathode, and this terminology will be used throughout the following sections. This certainly causes confusion when compared with typical SOFC nomenclature such as using “anode supported cell (ASC)” to indicate a cell with a nickel-yttria stabilized zirconia (Ni-YSZ) support, which in electrolysis mode is in fact the cathode. Perhaps calling the oxidizing and reducing atmosphere electrodes the “positive” and “negative” electrodes would avoid this confusion, but such terminology is not yet widely adopted.

2.1 Oxide-conducting MS-SOECs

The use of oxide-conducting MS-SOECs for steam electrolysis is a natural outgrowth of long-standing MS-SOFC development programs, and the first modern report was published more than a decade ago [37]. Steam/CO_2 co-electrolysis and CO_2-electrolysis have also been investigated. The most recent work from each group is summarized in Table 1. The electrolyte is either deposited on a pre-sintered support by plasma spray, pulsed laser deposition (PLD), or physical vapor deposition (PVD), or it is applied to the green support by tape casting or slurry coating and then co-sintered. These approaches have been compared in detail previously in the context of MS-SOFC development [14-16]. In all cases, Ni is a primary constituent of the cathode. Oxidation of Ni in high steam content conditions (especially at the stack inlet) is a concern, as the volume expansion upon oxidation will strain the adjacent electrolyte layer. Infiltrating small Ni particles into a porous electrode scaffold, or using an alternative ceramic cathode with low- or no-Ni content are effective approaches to impart redox tolerance for MS-SOFCs [13, 19], and are expected to be viable for MS-SOECs as well. $La_{0.6}Sr_{0.4}Co_{0.2}Fe_{0.8}O_3$ (LSCF) is a common choice for anode catalyst, but a variety of other compositions have also been used effectively. To avoid rapid oxidation, the metal support must not be exposed to air above ~900°C, and this limits the anode firing temperature to be much lower than the 1100 to 1200°C typically used for ASCs. This impacts anode performance and mechanical integrity. One approach to mitigate this limitation is the use of infiltrated catalysts, which require lower processing temperature. This is a common approach for MS-SOFCs, and has been utilized for some of the MS-SOECs discussed here [30-32].

Reference	Support	Cathode	Electrolyte	Anode	Electrolyte Processing	Active area cm^2	Electrolysis Reactant	Performance conditions T, H_2O/H_2 ratio	ASR Ohm cm^2	Current Density A cm^{-2}	Voltage V	Durability conditions T, H_2O/H_2, A cm^{-2}	Durability test time h	Degradation % kh^{-1}
[37]	Plansee IT11 SS	Ni-YSZ	YSZ	LSM	Plasma spray	12.50	H_2O	800°C, 30/70	0.45	0.75	1.30	800°C, 43/57, 0.3	2027	3.2
[41-42]	Plansee ITM SS	Ni-LST/GDC	YSZ/CGO	LSCF	Dip coat and PVD	16.00	H_2O	750°C, 80/20	0.40	0.75	1.15	750°C, 80/20, 0.25	120	13.7
[30]	430L SS	Ni-SDC	SSZ	Nd-NNO	Tape cast, sinter	0.35	H_2O	700°C, 50/50	0.31	1.06	1.30	600°C, 30/70, 0.166	330	19.3
[32]	P434L SS	Ni-SDC	SSZ	LSCF-SDC	Tape cast, sinter	3.00	H_2O	700°C, 50/50	0.80	0.41	1.30	700°C, 50/50, 0.33	1000	16.1
[46]	NiMo	Ni-YSZ/GDC	LDC/LSGM/LDC	SDC-SSC	Not reported	81.00	H_2O	800°C, 90/10	0.18	0.40	0.95	–	–	–
[48-47]	Ni-YSZ/430 SS sheet	Ni-YSZ	YSZ	LSCF	Slurry coat, sinter	0.64	H_2O/CO_2	800°C	1.10	0.65	1.40	800°C, NA, 0.8	300	160.0
[52]	Ni-Fe (9:1)	Ni-Fe (9:1)	LSGM/SDC	SSC	PLD	–	CO_2	700°C	0.23	3.00	1.45	–	–	–
[8]	430 SS mesh	Ni-YSZ	YSZ	LSCF	Plasma spray	1.75	CO_2	800°C	12.40	0.07	1.45	–	–	–

Table 1. Summary of oxide-conducting MS-SOEC studies. The supports are sintered porous structures unless indicated otherwise. All used air on the anode side, except for [8] which used nitrogen. In many studies, performance at various conditions were reported, and a single representative point is shown here. For cases where the degradation rate was not stated in the original work, it was estimated from continuous operation data after any initial transients were complete.

The performance of the MS-SOECs is moderate, with most displaying area-specific resistance (ASR) in the approximate range 0.2 to 1 Ohm cm^2. This can be compared to 0.15 Ohm cm^2 at 750°C for a high-performing example of ASC-based SOEC [38]. A reasonable goal is <0.45 Ohm cm^2, providing around 0.75 A cm^{-2} at 1.3 V in the case of steam electrolysis. ASR appears to be the most convenient metric for comparison between different cells, because there is no consistency in operating temperature or steam content (and therefore OCV). It is recommended in future work to report the performance at 50/50 H_2O/H_2 and the thermoneutral voltage as a standard for benchmarking comparison. The degradation rates demonstrated so far are much too high for commercial application. All are greater than 10% kh^{-1}, with the exception of the early plasma-sprayed cell (3.2% kh^{-1}) [37]. This can be compared to 0.4% kh^{-1} degradation reported for ASC-type SOECs [38], and 0.14% kh^{-1} reported for MS-SOFCs [39]. Detailed evaluation of MS-SOEC degradation phemonena has only been undertaken in two cases [32, 37]. Clearly, identifying degradation modes and improving durability should be key focus areas for future MS-SOEC efforts.

There does not appear to be a standard steam/hydrogen ratio for oxide-conducting MS-SOEC testing, but 50/50 can be recommended as a starting point. Low steam utilization conditions are also of interest, as stainless steel is expected to oxidize more quickly at higher steam content as discussed below in Section 3.1. Air is the oxidant atmosphere of choice due to the ease of implementing it in a lab setting, although

nitrogen flush has also been used in one case [8]. In all cases so far, long-term operation was conducted galvanostatically at current density ranging from 0.166 to 0.8 A cm^{-2}. It is recommended to also examine potentiostatic operation in the future, as the choice of operating voltage determines whether endothermic, exothermic, or thermoneutral conditions prevail.

Steam electrolysis

Steam electrolysis has been demonstrated with MS-SOECs utilizing a variety of cell fabrication approaches. The earliest effort by the German Aerospace Center (DLR) used plasma spray to deposit Ni-YSZ cathode, YSZ electrolyte, and (La,Sr)MnO_3 (LSM) or LSCF anode on a pre-sintered stainless steel support, Fig. 2 [37, 40]. A $La_{0.7}Sr_{0.15}Ca_{0.15}CrO_3$ barrier layer was also deposited between the support and Ni-YSZ cathode to prevent interdiffusion of Ni and Fe/Cr. A cell was characterized at 800°C with various steam:hydrogen ratios for 394 h, then switched to continuous electrolysis for an additional 2027 h using 43/57 H_2O/H_2 and air. This remains the longest MS-SOEC operation reported in the literature to date. The average degradation rate was 3.2% kh^{-1}, which is high relative to state of the art ASC electrolysis cells, but significantly lower than all of the other MS-SOECs reported to date. Intermittent EIS was used to analyze the degradation modes. A small increase in ohmic impedance (60 mOhm cm^2) was ascribed to oxidation of the stainless steel support, which was confirmed in post-mortem scanning electron microscope (SEM) images, Fig 2b. A large increase in electrode polarization (130 mOhm cm^2) was observed during the initial cell characterization period, during which temperature and steam content were varied, and switching between fuel cell and electrolysis modes occurred. A smaller (30 mOhm cm^2) additional increase in electrode polarization was observed after long-term electrolysis operation. Post-mortem SEM and energy-dispersive spectroscopy (EDS) analysis revealed Ni coarsening in the cathode, but Ni and Fe/Cr interdiffusion were not observed, suggesting the diffusion barrier layer was effective. Operation of cells

contacted by a coated metallic interconnect with and without a Pt mesh between them indicated that contact resistance is a significant issue, but the presence of the metallic interconnect did not introduce additional degradation. Apparently, the coating was effective at blocking Cr transport from the interconnect to the anode.

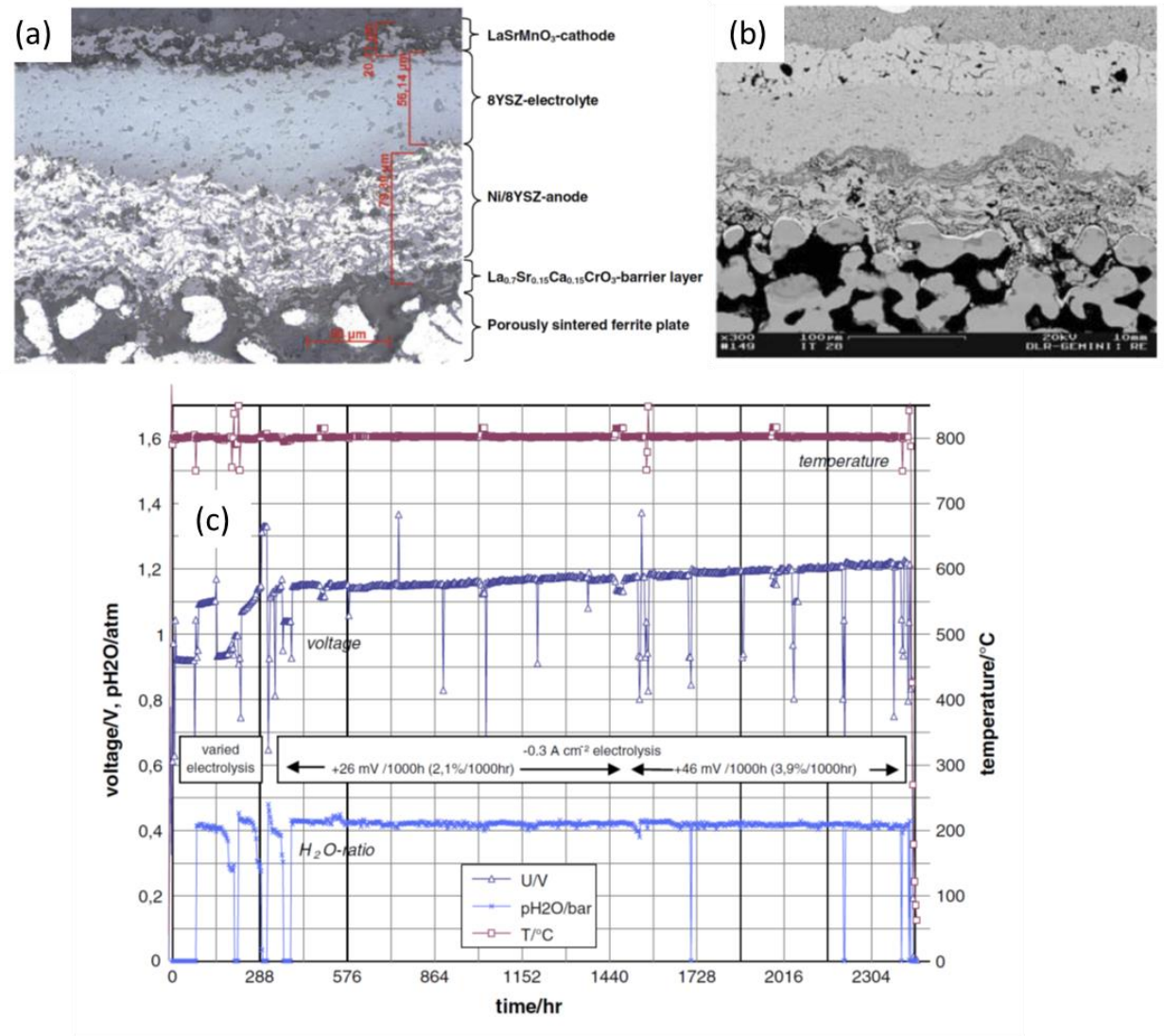

Figure 2. Long-term operation of oxide-conducting MS-SOEC prepared by plasma spray of YSZ onto stainless steel support. Cell structure (a) before operation and (b) after steam electrolysis operation. (c)

Temperature, voltage, and steam ratio during operation. Reproduced with permission from Reference [37].

DLR also used PVD to apply dense CGO/YSZ bi-layer electrolyte to a pre-sintered stainless steel substrate [41, 42]. (La,Sr)TiO_3 (LST)-GDC cathode and LSCF anode were applied by screen printing and firing. Ni was introduced to the cathode by infiltration. The open-circuit voltage (OCV) for 80/20 H_2O/H_2 and air was 50 mV lower than expected, likely due to small defects in the electrolyte layers. Performance was significantly activated (improved with higher current density) in electrolysis mode, but not so in fuel cell mode. After short-term operation for 120 h, the polarization impedance did not change, but significant degradation of 13.7 % kh^{-1} was caused by an increase in ohmic impedance. Post-mortem evaluation suggests oxidation of the stainless steel support in high steam condition and delamination of the weakly-bonded LSCF anode are likely culprits.

The other standard fabrication approach pioneered in the early 2000's [43, 44], is co-sintering the stainless steel support and zirconia electrolyte, followed by infiltration of the catalysts. This approach was first demonstrated in electrolysis mode by the Shanghai Institute of Ceramics, Chinese Academy of Sciences (SICCAS), Fig. 3a-b [30]. A 430L stainless steel support, 430-YSZ cathode backbone, Sc-stabilized zirconia (SSZ) electrolyte, and SSZ anode backbone were tapecast, laminated, and co-sintered in reducing atmosphere. Ni-SDC and Nd_2O_3-Nd_2NiO_4 catalysts were then infiltrated multiple times in air to the cathode and anode sides, respectively, and calcined at 800°C in situ before operation. The electrolysis polarization curve displayed curvature due to activation at 650°C, but was fairly linear in the range 700 to 800°C. At 750°C and above, it displayed concentration polarization, the extent of which changed dramatically with steam/hydrogen ratio, and curtailed the current density available at 1.3 V for steam content of 30% and below. The catalyst particle size was in the range of approximately 50 to 200 nm, and the catalyst

structure did not appear to change visually after 146 h electrolysis operation at 650°C. Despite this particle size stability, during 330 h operation at 600°C the performance improved significantly during an initial ~100 h transient, then degraded continuously during the remainder of the operating time. Detailed post-mortem analysis was not performed.

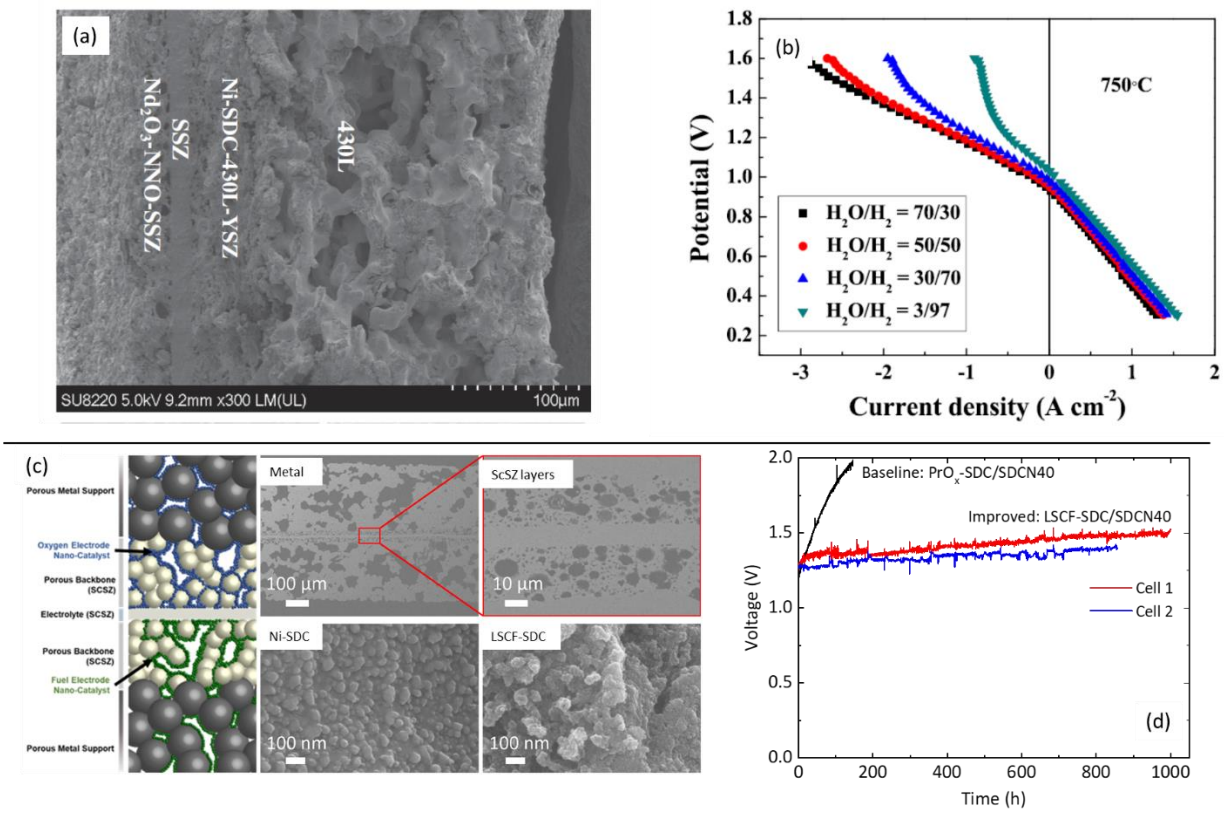

Figure 3. Steam electrolysis with oxide-conducting MS-SOECs prepared by co-sintering SSZ with stainless steel support, and catalyst infiltration. (a) Cross-section SEM image and (b) performance data for a cell with Ni-SDC cathode and Nd_2O_3-NNO anode catalysts, reproduced with permission from Reference [29]. (c) Schematic and SEM image and (d) durability data for a cell with Ni-SDC cathode and PrO_x-SDC or LSCF-SDC anode catalysts, reproduced with permission from Reference [31].

The co-sintering approach is also used by LBNL to fabricate a symmetric-structured MS-SOEC with porous metal supports on both sides, Fig 3c-d. The symmetric structure provides good mechanical strength, enables welded electrical connections on both sides, and maintains flatness even if expansion/contraction of the individual layers is mismatched. Thus, differences between metal and ceramic sintering rates during fabrication, and thermal expansion rates during start-up, do not cause distortion or warping of the cell. Early work focused on optimization of the infiltrated catalysts for electrolysis operation [31]. LSM, LSCF, and Pr_6O_{11} oxygen catalysts were screened, and Pr_6O_{11} provided the highest performance. Addition of Sm-doped ceria (SDC) to the oxygen catalyst improved performance, attributed to an increase in triple phase boundary length and ionic conductivity of the composite catalyst. The Ni:SDC ratio on the steam electrode side was varied, and 60 vol% Ni provided the highest performance. Recent results indicate, however, that the catalysts chosen as optimal for performance do not provide adequate durability [32]. A cell with Pr_6O_{11}-SDC anode degraded quite rapidly (541% kh^{-1}). A lower-performing cell with LSCF-SDC anode and Ni-SDC (40 vol% Ni) cathode catalysts displayed much lower degradation rate (16.1% kh^{-1}) and was operated continuously for 1000 h, Fig 3d. Detailed post-mortem analysis revealed the degradation modes to be coarsening and Ni agglomeration of the steam catalyst (Ni-SDC), oxidation of the supports, and Cr poisoning on the oxygen catalyst (LSCF-SDC). Employing a stainless steel support on the air side is a fundamental limitation of this symmetric cell design, because it acts as a Cr source in close proximity to the oxygen catalyst. Coating the support suppressed Cr migration in fuel cell mode [45], and should be implemented for electrolysis mode in the future.

Aside from stainless steel, NiMo has also been used as a support material [46]. A cell with the layer configuration NiMo/Ni-YSZ/Ni-GDC/LDC/LSGM/LDC/SDC-SSC was operated at 800°C with 90:10 H_2O/H_2 and air. Details of cell preparation were not provided, but presumably the layers were deposited on a pre-formed NiMo substrate by atmospheric plasma spray deposition, as reported by the same institution

previously for MS-SOFC development [47]. The performance was excellent, providing 0.35 A cm^{-2} at 0.96 V.

Steam/CO_2 co-electrolysis

Though not technically a metal-supported cell, mechanical properties can be improved by directly bonding an ASC to a metal interconnect sheet. Such a cell was used to demonstrate H_2O/CO_2 co-electrolysis to produce syngas [48, 49]. The performance was substantially worse than a similar ASC which was not bonded to the interconnect and degradation was rapid, partly because the LSCF oxygen electrode was sintered at 1100°C for the free-standing ASC, but only sintered at the operating temperature (800°C) for the cell bonded to the interconnect. Nevertheless, co-formation of H_2 and CO was successfully demonstrated.

CO_2 electrolysis

Ishihara's group at Kyushu University has explored CO_2 electrolysis using $La_{0.9}Sr_{0.1}Ga_{0.8}Mg_{0.2}O_3$ (LSGM) electrolyte, motivated by industrial re-use of CO_2 to provide CO as a fuel, and O_2 for combustion [50-52]. Early work used electrolyte-supported cells to identify NiFe (9:1) as a high performing alloy cathode, which can be further improved by addition of $La_{0.6}Sr_{0.4}Fe_{0.8}Mn_{0.2}O_3$ (LSFM) or other ceramic oxide ion conductors [50, 51]. Significantly higher performance was achieved recently by switching to a metal-supported design utilizing a much thinner 10 μm thick electrolyte layer and SSC anode deposited by PLD, Fig. 4 [52]. NiFe (9:1) serves as both the support and cathode, and is prepared as a nearly dense NiO-Fe_2O_3 substrate that enables PLD deposition of the SDC/LSGM bilayer electrolyte directly onto the smooth substrate surface. The substrate is later reduced, introducing sufficient porosity. The polarization curves obtained at 500 to

700°C with CO_2 and air are characterized by two regions. Below the theoretical OCV (0.937 V) low current density is observed, speculated to arise from electrochemical pumping of impurity oxygen in the CO_2 stream. Above ~0.9 V, higher current density is observed and the polarization appears to include activation overpotential at 500°C but becomes almost linear at 700°C, where approximately 3 A cm^{-2} is obtained at 1.45 V. A cell with $Sm_{0.5}Sr_{0.5}CoO_3$ (SSC) applied by screen printing instead of PLD demonstrated near-100% Faradaic efficiency, suggesting the LSGM was gas-tight and did not display electronic conduction.

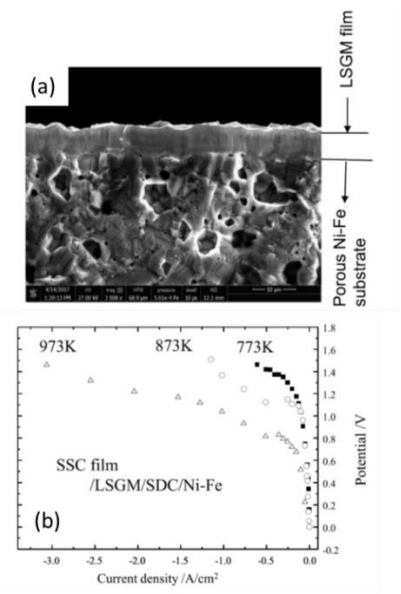

Figure 4. LSGM-based oxide-conducting MS-SOEC prepared by PLD on NiFe support. (a) Cross-section image and (b) polarization curves for CO_2 electrolysis. Reproduced with permission from Reference [50].

CO_2 electrolysis was also demonstrated with a YSZ-based cell deposited by plasma spray onto a 430 stainless steel mesh support [8]. The electrolyte was ~200 μm thick and quite porous, resulting in low cell performance. Leakage through the electrolyte also caused low Faradaic efficiency. Nevertheless, the cell displayed good mechanical durability, and reaction between adjacent layers was not observed after fabrication or operation. A process model, with the MS-SOEC used to recycle carbon through an iron-

making furnace, was analyzed to determine the system-level electrical and heat flows required for an overall 30% reduction of CO_2 emissions.

2.2 Proton-conducting MS-SOECs

Proton-conducting SOECs operate at lower temperature than oxide-conducting cells, and produce dry hydrogen [12, 53]. These differences may become critical advantages for MS-SOECs, once challenges with fabrication of dense proton-conducting electrolyte on porous metal supports are overcome. The lower operating temperature is more compatible with steam or waste heat available from industrial or geothermal facilities, and will reduce oxidation rate of the metal support as discussed below in Section 3. If the metal support is located on the dry hydrogen side, it may further reduce oxidation rate and potentially enable the use of low-cost support materials that do not form a protective oxidation scale. Metal-supported cells are more mechanically robust than ceramic-based cells, and are expected to tolerate large pressure differences across the cell. Precise matching of the steam and hydrogen side pressures is not necessary. Electrochemical compression of hydrogen is therefore possible, producing a dry, pressurized hydrogen product without the expense and complication of separate mechanical pressurization and steam-condensation steps.

The development of proton-conducting MS-SOECs is nascent. Performance and durability data are not yet available, although some cells have been analyzed with EIS at open-circuit conditions, as discussed below. Therefore, this section focuses on various cell architecture and fabrication techniques that are under

development. In certain cases, cells that have been tested only in SOFC conditions are included because they are anticipated to be promising for SOEC operation as well.

Deposition of electrolyte onto pre-formed support

$BaZr_xCe_yY_{1-x-y}O_3$ (BZCY) and other proton-conducting ceramics are difficult to sinter in the 1300 to 1400°C temperature range and reducing atmosphere required for sintering stainless steel supports. Therefore, the most successful approaches so far involve deposition of a dense ceramic electrolyte layer onto a preformed metal support using PLD, sputtering, or spray deposition techniques. PLD is the most commonly used so far, however the suitability of PLD for high-throughput low-cost manufacturing needs further clarification.

Electron-conducting and hydrogen-permeable Pd-based solid metal hydrogen electrodes provide a smooth, dense surface for deposition of a thin defect-free electrolyte layer. Radio frequency (RF) sputtering was used to deposit a 1 μm thick $BaCe_{0.8}Y_{0.2}O_3$ (BCY) film onto 30 μm thick $Pd_{0.8}Ag_{0.2}$ alloy sheet, followed by screen printing an LSCF oxygen electrode [54]. The cell was operated with dry hydrogen and wet oxygen, providing almost 1.2 W cm^{-2} in fuel cell mode at 600°C. To save cost, a similar approach was taken with a much thinner dense 5 μm Pd layer plated onto a thick porous stainless steel support [55]. A 1.2 μm $SrZr_{0.8}Y_{0.2}O_3$ (SZY) electrolyte and 0.1 μm LSCF oxygen electrode were deposited onto the Pd surface by PLD. Fuel cell mode operation was demonstrated at a very low temperature of 400°C. While the preparation of these cells appears straight-forward and the performance is impressive, the high cost

of the Pd membrane must be addressed, possibly by replacement with other hydrogen permeable materials.

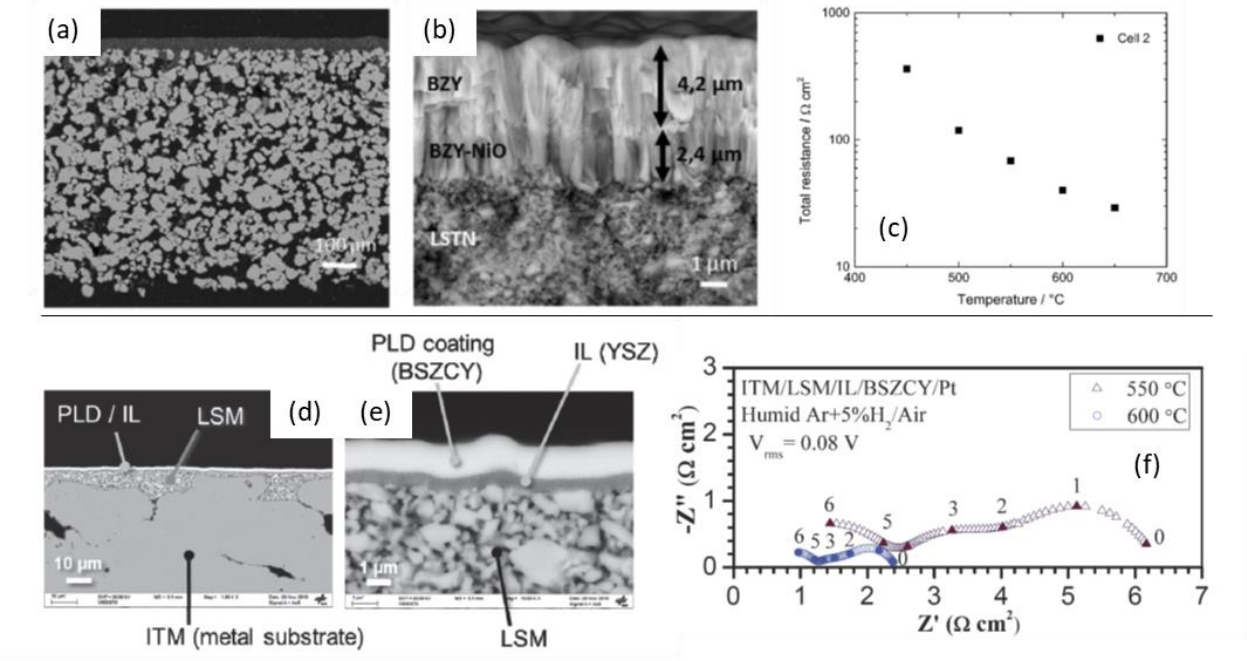

Figure 5. BZY-based proton-conducting MS-SOECs prepared by PLD onto stainless steel supports, tested under steam electrolysis atmospheres. (a, b) SEM cross-section images of BZY-based cell, and (c) total EIS impedance at OCV, reproduced with permission from Reference [54]. (d,e) SEM cross-section images of BSZCY-based cell, and (c) impedance spectra at OCV, reproduced with permission from Reference [56].

PLD deposition of a high-quality BZCY electrolyte onto a porous electrode is more challenging. Significant progress in recent years has been led by SINTEF and the University of Oslo (Norway) with collaboration by DLR (Germany) [56-59]. Their approach utilizes a micro- or nano-porous interlayer to cover over the large pores of the stainless steel metal support, followed by PLD deposition of $Ba(Zr,Y)O_3$ (BZY) electrolyte. Various interlayers were considered, and it was found that BZY-Ni sintered poorly and therefore did not provide a good surface for electrolyte deposition, and CeO_2 was associated with short-circuiting during

cell operation [57]. $La_{0.5}Sr_{0.5}Ti_{0.75}Ni_{0.25}O_3$ (LSTN) was selected as the most promising interlayer, and developed further, Fig 5a-c [56]. The metal support is sintered, then coated with LSTN to smooth over the surface pores. BZY-NiO electrode and BZY electrolyte layers are then deposited by PLD, using conditions optimized for each layer. Significant optimization effort for each layer resulted in a smooth interlayer with no obvious cracking and a continuous dense electrolyte layer. This half-cell was operated at 450 to 650°C with a Pt top electrode exposed to wet argon, and dry hydrogen on the BZY-Ni side. The total impedance was 40 Ohm cm^2 at 600°C, much higher than expected for a thin electrolyte. OCV was not reported, so the gas-tightness of the electrolyte cannot be assessed. Performance of the cell was thought to be limited by large grain boundary resistance in the electrolyte due to small grains, or possibly poor contact with the LSTN substrate surface. To improve conductivity of the electrolyte, Ag heat transfer paste was inserted under the cell during PLD deposition to improve BZY crystallinity, and a post-deposition annealing step was added [59]. The annealing step introduced cracking in the electrolyte, thought to arise from coefficient of thermal expansion (CTE) mismatch between the BZY and other cell layers. A new Sr- and Ce-doped BSZCY composition with increased CTE was developed, and this enabled annealing around 1200°C with minimal cracking. OCV of 1.106 V was achieved at 400°C with air and humid hydrogen, indicating a relatively defect-free electrolyte layer was achieved. Cell performance was not reported. A modified cell structure based on the same approach was developed recently, Fig 5d-f [58]. An LSM diffusion barrier layer and YSZ interlayer were applied to an intermediate-temperature-metal (ITM) support and sintered at up to 950°C. BZY or Sr,Ce-doped BZY (BSZCY) electrolyte was then deposited by PLD to a thickness around 1 μm. The half-cell was operated with Pt electrode on top, with wet hydrogen and air. It is unclear if the LSM survived these conditions, as it is expected to decompose in hydrogen fuel atmosphere. The OCV was too low to obtain a polarization curve, but electrochemical impedance spectroscopy (EIS) was obtained at OCV condition. At 550°C, assuming the ohmic portion was due to only the electrolyte, an electrolyte conductivity of 10^{-4} S cm^{-1} was estimated. This is more than 2 orders of magnitude lower than

the conductivity expected for BZY-type materials [60]. In summary, continuous optimization effort has achieved a good understanding of the processing requirements for PLD deposition of BZY onto a porous stainless steel support, and successful operation of a functional cell is anticipated in the near future.

Suspension plasma spray (SPS) deposition is proposed as a lower-cost alternative to PLD for BZCY-type electrolyte [61]. Cost modeling suggests cell cost below \$0.10 cm^{-2} can be achieved with this technique. BZCY was deposited by SPS onto a substrate of Ni-BZCY (60 μm thick) pre-sintered onto a porous stainless steel support. Defects in the electrolyte due to erosion of the Ni-BZCY layer during SPS deposition caused low OCV in the range 0.15 to 0.4 V, which limited the electrolysis current at 1.4 V to 0.25 A cm^{-2}. Further improvements in the deposition process and Ni-BZCY/metal support substrate are ongoing. In an earlier related effort, reactive spray deposition technology (RSDT) was used to deposit a Ni-BZY/BZY/LSCF structure on a pre-sintered 430 stainless steel porous support [62]. The maximum temperature the support experienced during deposition was 855°C, avoiding rapid oxidation. Performance was not reported.

Co-sintering the electrolyte and metal support

Co-sintering, in which the metal support, electrolyte, and one or more electrode layers are sintered together in a single step, is a desirable approach for fabricating proton-conducting MS-SOECs. The electrolyte and electrode layers can be formed via tape-casting, screen-printing, or other low-cost and scalable ceramic processing techniques. Sintering can also yield a dense micron-scale grain structure in the electrolyte, providing high conductivity and mechanical strength. While this approach is very successful for oxide-conducting MS-SOECs (Section 2.1), its application to proton-conducting materials is much more challenging.

A survey of various families of ceramic proton-conductors found that many are not compatible with the sintering conditions required for stainless steel supports, namely 1300 to 1450°C in reducing atmosphere [63]. The pyrochlores $La_{1.95}Ca_{0.05}Zr_2O_7$ (LCZ) and $La_2Ce_2O_7$ (LCO) decomposed under these sintering conditions. Three perovskites were shown to survive sintering in reducing atmosphere: $Ba_3Ca_{1.18}Nb_{1.82}O_9$ (BCN), $SrZr_{0.5}Ce_{0.4}Y_{0.1}O_3$ (SZCY), and $BaZr_{0.7}Ce_{0.2}Y_{0.1}O_3$ (BZCY). These faced other challenges, including evaporation of Ba and Sr during sintering, and reaction with Cr and/or Si in the stainless steel to form inert phases. BZCY and SZCY did sinter successfully, however, but complete densification of BZCY was not achieved due to the low sintering temperature relative to typical sintering of BZCY in air around 1500°C. The one material that appeared to be easily compatible with co-sintering of stainless steel was the doped ortho-niobate $La_{0.99}Ca_{0.01}NbO_4$ (LCN). A dense LCN electrolyte and porous LCN electrode backbone were deposited on a P434L stainless steel support by brush-painting and aerosol spray deposition, Fig 6a-b. After co-sintering, the LCN electrolyte was dense with well-formed grains in the 1 to 5 μm size range. The porous support and LCN electrode were infiltrated with Ni-SDC catalyst, and a Pt paste electrode was painted on the exposed electrolyte surface. EIS was performed in the range 450 to 750°C, with air and wet hydrogen. The cell performance was limited by the low conductivity of LCN, and a high impedance of around 50 Ohm cm^2 was observed at 600°C. While this was considered to be the first demonstration of a co-sintered proton-conducting MS-SOC, the low performance did not justify further development.

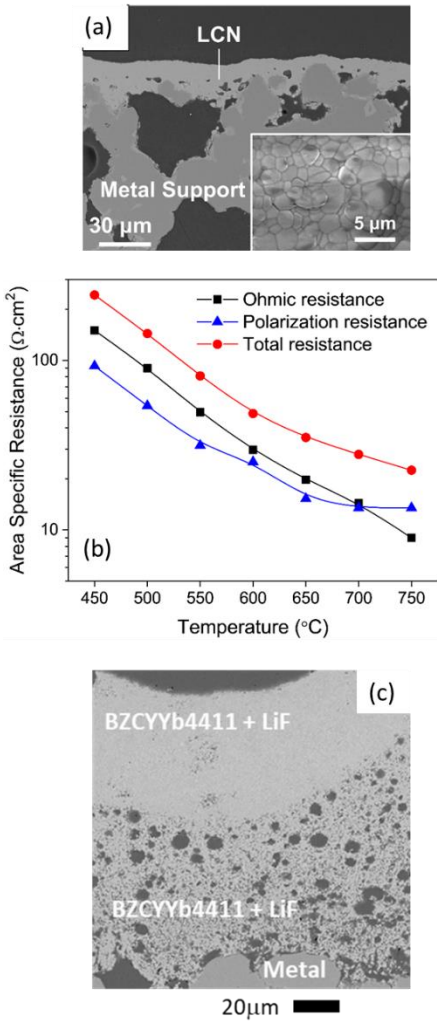

Figure 6. Proton-conducting MS-SOECs prepared by co-sintering the electrolyte and stainless steel support. (a) SEM cross-section and electrolyte surface (inset) images and (b) EIS impedances for a cell with LCN electrolyte, reproduced with permission from Reference [61]. (c) SEM cross-section image of a cell with BZCY-based electrolyte and LiF sintering aid, reproduced with permission from Reference [62].

Despite the challenges associated with co-sintering, BZCY was selected for further development due to its high conductivity. Three specific problems with co-sintering were identified: evaporation of Ba during sintering, which is accelerated by reducing atmosphere relative to air; marginal sintering at 1450°C or lower, as required to avoid melting or over-densification of the metal support; migration of Cr and Si into

the electrolyte, forming barium-silicate and -chromate [64]. The last issue was partially mitigated by using stainless steel with very low Si content, and inserting a doped ceria barrier layer between the metal support and BZCY layers. It was recognized that all of the co-sintering challenges are temperature-dependent, and might be mitigated by lowering the sintering temperature required for densification of BZCY. The use of sintering aids to achieve this goal was evaluated. NiO, ZnO, and Co_3O_4 are widely used as sintering aids for BZCY in air, but were not effective in reducing atmosphere. Addition of 2w% LiF dramatically lowered the sintering temperature, presumably *via* a liquid-phase sintering mechanism as the melting point of LiF is 848°C. A half-cell with metal support, porous BZCY electrode scaffold, and dense BZCY electrolyte was co-sintered at 1300°C using LiF in both ceramic layers, Fig 6c. The electrolyte contained no Cr and minimal Si, but was cracked due to shrinkage mismatch between the metal and ceramic layers. This prevented preparation and operation of a full cell. Further optimization of the sintering aid and barrier layer approaches is ongoing.

In an attempt to overcome challenges with sintering in reducing atmosphere, $BaZr_{0.1}Ce_{0.7}Y_{0.1}Yb_{0.1}O_{3-\delta}$ (BZCYYb) electrolyte was sintered in air on a NiO support, which was later reduced to Ni during cell operation [65]. NiO-BZCYYb electrode and BZCYYb electrolyte layers were dip coated onto the tubular NiO support. During sintering in air at 1450°C, significant grain growth of the support occurred. This led to cracking of the electrolyte during reduction of the support to Ni metal, reminiscent of the common issue of cracking during redox cycling of ASCs. The cells were tested in fuel cell mode, but the cracked electrolyte resulted in low OCV (0.88 V at 700°C). Addition of a small amount of YSZ to the Ni support layer improved the microstructure, but did not eliminate electrolyte cracking. Other concerns with Ni support also remain, including cost, redox cycling intolerance, and thermal expansion mismatch with BZCY-type electrolytes.

3. Oxidation of metal supports

Oxidation of metal supports in oxygen atmosphere or high-steam atmospheres is a concern for cell degradation and mechanical integrity, Fig 7a. Oxidation is a well-studied phenomenon of dense stainless steel interconnects for SOFC stacks and porous supports for MS-SOFCs, however few studies have assessed oxidation behavior specifically for SOEC operating conditions. In both anode and cathode environments, stainless steel oxidizes to form a protective Cr-based oxide scale that is electronically conductive, although less so than the bulk metal. As the scale grows, electronic resistance increases and can contribute significantly to the total area-specific resistance (ASR). Spallation can occur for scale thickness above a few micrometers, which breaks the electronic pathway, increases the oxidation rate, and eventually leads to mechanical failure of the stainless steel. The oxidation rate is influenced by operating temperature, stainless steel composition, and the presence of protective coatings. Critically, the oxidation rate is also sensitive to the oxygen partial pressure and steam content in the operating environment, and these may be quite different for SOEC operation compared to the SOFC operation conditions used for most previous oxidation studies, Figs 1 and 7. High steam content at the stack inlet (low steam utilization conditions) is a particular concern, as it leads to dramatically higher oxidation rate [66-68].The relevant conditions for oxide-conducting SOECs are dry oxygen (or oxygen-enriched air) and H_2/H_2O with a high steam content around 650 to 800°C, and for proton-conducting SOECs are dry hydrogen and O_2/H_2O with a high steam content around 500 to 700°C, Fig 1. MS-SOEC designs have used a single metal support on the hydrogen-containing side [30, 37] or metal support on both sides [31, 32], and MS-SOECs with metal support on only the oxygen side may find application in the future. Therefore, all of the atmospheres mentioned above are of interest for oxidation studies relevant to MS-SOECs.

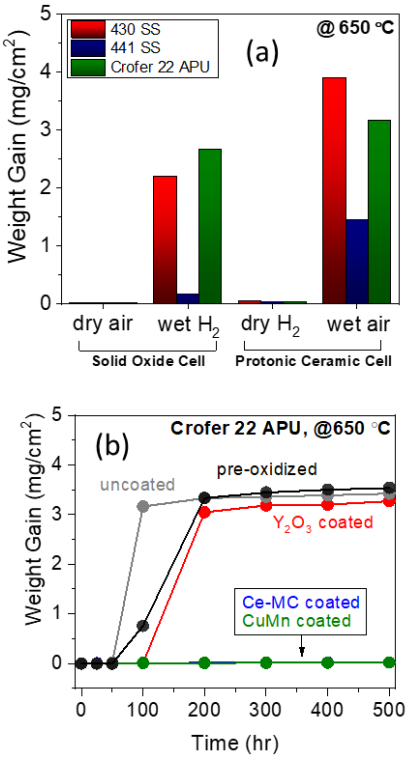

Figure 7. Oxidation of dense stainless steels at 650°C. (a) Comparison of oxidation behavior in various atmospheres relevant to electrolysis with oxide-conducting or proton-conducting electrolytes (see Fig 1). (b) Oxidation behavior of Crofer 22 APU in wet air, pre-oxidized (black), with various coatings (red, blue, green), or uncoated (gray). Reproduced with permission from Reference [76].

Oxidation of porous stainless steels is moderately well studied, and the numerous studies of dense interconnects can provide some guidance. Critical differences for porous supports are that the surface area-to-volume ratio is large, so Cr depletion from the bulk may occur for supports with fine structure [69], and deposition of dense coatings inside the support structure is not as straightforward as the line-of-sight coating methods used for dense interconnect surfaces. However, the general oxidation phenomena observed for porous stainless steel supports are qualitatively similar to those observed for dense interconnects. In particular, oxidation kinetics are parabolic after an initial short-term transient, the oxidation rate shows an Arrhenius dependence on temperature, and coatings can dramatically reduce the

oxidation rate [69, 70]. Therefore, the results of dense interconnect oxidation studies are expected to broadly apply to porous supports. An additional complication for porous materials is the growth of the scale into the porespace, which can close off pores thereby degrading gas transport pathways through the support [71, 72].

3.1 Oxidation in oxide-conducting SOEC conditions

Ex-situ oxidation

For oxide-conducting SOECs, the relevant atmospheres are dry oxygen, and steam with hydrogen, Fig 1b. A few studies considering oxidation of stainless steel interconnects in electrolysis conditions indicate that oxidation in pure oxygen is similar to air, and the mechanism and scale composition are not significantly affected. The oxidation rate in oxygen was found to be the same or slightly higher than in air at 850 to 900°C, although the grain size of the oxide scale was larger for oxygen [73, 74]. Importantly, Cr evaporation in dry oxygen was slower than in moist air, and it is reasonable to assume that Cr poisoning in oxide-conducting SOECs will be slower than typically observed for SOFCs with moist air.

The high steam content associated with steam electrolysis exacerbates oxidation. Steam with a small hydrogen content is found at the inlet of oxide-conducting SOECs, and at the outlet of SOFCs with high fuel utilization. This scenario has been studied for oxidation resistance of porous stainless steels, and the results are expected to be applicable to SOEC operation. Uncoated porous Fe78-Cr22 stainless steel was exposed to wet hydrogen intended to represent 90% fuel utilization and also represent 10% steam utilization in electrolysis mode (9:1 H_2O:H_2) at 850°C for 500h [75]. A significant extent of oxidation occurred and a 2 to 4 μm thick scale developed throughout the structure, indicating that high steam content is a concern for stability of the support, Fig 8a. A porous sample coated with Mn-based spinel and

Ni-CGO anode catalyst displayed minimal oxidation after 500h, suggesting that coatings are an effective approach to mitigate the risk of high-steam operation, Fig 8b. Similar samples were oxidized at 650°C and displayed very thin scales, underscoring the role of operating temperature in durability of the metal support, although areas with fine metal particles still experienced rapid oxidation in the high-steam condition. Lower steam content can still be problematic. Porous stainless steel with 20.6% Cr was exposed to wet hydrogen (1:2 H_2O:H_2) and a protective scale did not form at 600 and 700°C, leading to breakaway oxidation (discussed in Section 3.2), Fig 8c [76]. Application of a $La(Mn,Co)_{0.8}O_3$ coating enabled formation of a protective scale, resulting in slow parabolic scale growth, Fig 8d.

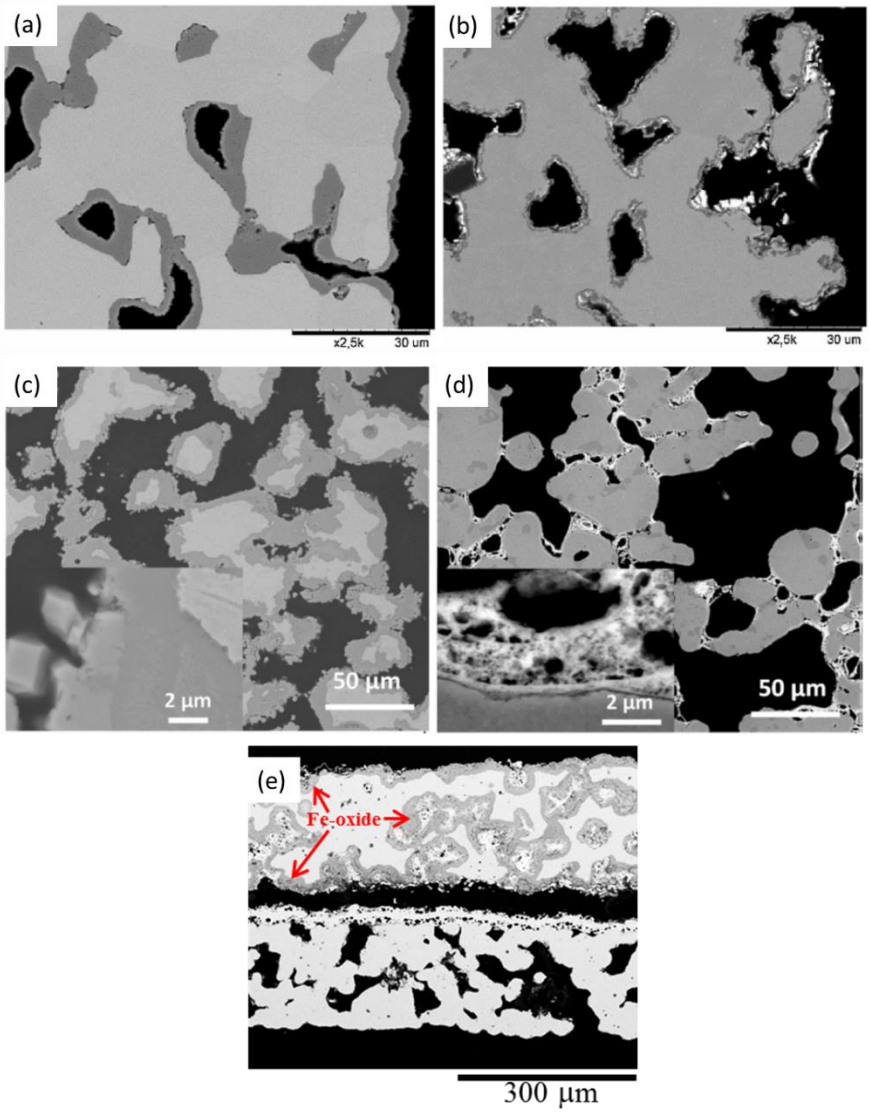

Figure 8. Oxidation of porous stainless steel supports. (a-e) Cross-section SEM images. Fe78-Cr22 stainless steel (a) uncoated or (b) coated with Ni-CGO and exposed to 9:1 H_2O/H_2 for 500 h at 850°C. Reproduced with permission from Reference [73]. Stainless steel (20.6% Cr) (c) uncoated and (d) coated with $La(Mn,Co)_{0.8}O_3$ after exposure to 1:2 H_2O:H_2 for ~200 h at 700°C. Reproduced with permission from Reference [74] (e) Breakaway oxidation observed on P434L stainless steel with Pr_6O_{11} coating after operation in fuel cell mode at 600°C. The delaminated and heavily oxidized stainless steel top layer was exposed to air. Reproduced with permission from Reference [79].

In-situ oxidation during MS-SOEC operation

Post-mortem evaluation of support oxidation after MS-SOEC operation has only been reported twice. A MS-SOEC with porous IT11 ITM alloy support (Plansee) was operated for more than 2000 h at 800°C with 43% H_2O-57% H_2 on the metal support/Ni-YSZ side, Fig 2 [37]. Ohmic impedance increased 60 mOhm cm^2, which was ascribed to minor oxidation observed on the metal support, Fig 2b. Total cell impedance increased 220 mOhm cm^2, so the oxidation caused a small but non-negligible portion of the total degradation. A MS-SOEC with porous P434L stainless steel supports on both sides was operated for 1000 h at 700°C with 50/50 H_2O/H_2 on the steam side and ambient air on the oxygen side, Fig 3d [32]. Oxidation was faster on the oxygen side, with about 1 μm scale thickness accumulated during operation, compared to about 0.2 μm for the steam side. Based on the limited results available to date, it appears oxidation in electrolysis mode is similar to that observed in fuel cell mode. A thin scale grows during operation and is expected to contribute to performance degradation via increased ASR, but catastrophic oxidation is not observed under normal operating conditions.

3.2 Oxidation in proton-conducting SOEC conditions

Ex-situ oxidation

For proton-conducting MS-SOECs, the relevant atmospheres are dry hydrogen, and steam with oxygen, Fig 1b. Sandvik Sanergy HT was suggested as an interconnect material for proton-conducting fuel cells. Dense sheets were found to have sufficient oxidation resistance at 700 to 900°C in air with 2.5% moisture [77]. Oxidization rate at the lower temperature and higher moisture content expected for state-of-the-art PCECs was not studied, however. Wang et al. produced the first study of stainless steel oxidation in

oxidizing environment with high steam content at intermediate temperature (450 to 650°C) relevant to PCEC, using dense coupons around 150 μm thick [78]. Oxidation in wet air (50% air, 50% H_2O) was found to be significantly more aggressive than ambient air (~1.5% H_2O), dry hydrogen (2.8% H_2, balance Ar), or wet hydrogen (2.8% H_2, 50% H_2O, balance Ar) for 430, 441, and Crofer 22 APU stainless steels, Fig 7. In wet air, all uncoated alloys displayed breakaway oxidation. Breakaway oxidation occurs when the rate of Cr consumption via oxidation is higher than the rate of Cr diffusion through the bulk of the metal to the surface, and leads to rapid formation of Fe-rich oxide scales [79]. Pre-oxidation to form a continuous chromia coating can prevent breakaway oxidation [68], however this was not found to be successful for exposure to wet air. Possibly this is due to enhanced Cr consumption *via* evaporation in wet air outstripping the rate of Cr diffusion through the bulk to the scale. Coating the stainless steel with common oxidation-suppressing coatings such as Cu-Mn-oxide or Ce-Mn-Co oxide prevented breakway oxidation, and lowered the oxidation rate to ~10^{-16} $g^2cm^{-4}s^{-1}$, which is certainly low enough to prevent oxidation-based failure of the device, Fig 7b.

Breakaway oxidation around 600°C

The intermediate operating temperature expected for proton-conducting MS-SOFCs is also a concern. Counterintuitively, as the operating temperature drops to around 600°C, oxidation rate can increase dramatically due to breakaway oxidation because the Cr diffusion rate is lower than the Cr oxidation consumption rate at this temperature. This is illustrated well by dual-atmosphere oxidation of dense 441 stainless steel sheets, for which oxidation at 700 and 800°C produced a normal protective Cr-based scale, but at 600°C rapid growth of Fe_2O_3 was observed [80]. Below 600°C, the oxidation rate becomes low enough that the Cr diffusion rate is once again sufficient to provide a protective scale. Breakaway

oxidation of porous P434L stainless steel was observed during fuel cell mode operation at 600°C on the air-side support, leading to device failure in less than 100 h [45]. Pre-oxidation extended the lifetime, but did not entirely solve the issue. Volume change of the support due to extensive breakaway oxidation caused delamination of the support from the cell leading to leakage and an associated drop in open circuit voltage, Fig 8e. Post-mortem SEM evaluation also revealed that the support pores were filled with Fe-oxide. A subsequent study of porous P434L oxidation in air at 600°C revealed that breakaway oxidation only occurs when the moisture content is above 3% [81]. This suggests the moisture content on the air side of the failed cell (Fig 8e) was higher than ambient (typically ~1.5%), most likely due to pinhole leaks in the electrolyte allowing hydrogen to burn and create additional steam on the air side. Pre-oxidation was sufficient to suppress breakaway oxidation for moisture content up to 50% in air. Breakaway oxidation was also observed at 600°C for an as-sintered support in wet hydrogen (H_2:H_2O 45:55), and likewise pre-oxidation prevented breakaway oxidation [81]. Similarly, breakaway oxidation was reported at 600°C in high steam content hydrogen (2% H_2-8% H_2O-90% Ar) for sintered stainless steel (22% Cr), and the application of a $La(Mn_{0.5}Co_{0.5})_{0.8}$-oxide coating completely suppressed breakaway oxidation [68]. Breakaway is not expected to be an issue on the dry-hydrogen side of a proton-conducting MS-SOEC due to the very low oxygen partial pressure, but this remains to be confirmed experimentally around 600°C. Also, any leakage of oxygen or steam to the dry-hydrogen side could cause breakaway oxidation.

These results suggest that it is preferable for a proton-conducting MS-SOFC to have a single porous metal support on the cathode (dry hydrogen) side, and if a metal support is used on the anode (wet oxygen) side it must be coated with a relatively dense coating to prevent breakaway oxidation.

3.3 Supports other than stainless steel

Stainless steel is by far the most common choice of support material for MS-SOFCs and MS-SOECs, but other metals have been used including NiMo and NiFe [46, 52]. These are not expected to form a protective scale, but they can be stable under certain conditions. NiFe did not oxidize in low steam content hydrogen (1:2.9 H_2O:H_2) at 750°C, but Fe_2O_3 was formed in high steam content (3.7:1 H_2O:H_2) although only a moderate impact on electrical conductivity was reported [82]. At even higher steam content relevant to oxide-conducting MS-SOECs, Ni is also expected to oxidize. This may be avoided by recirculating the exhaust gas to maintain higher H_2 concentration at the stack inlet, although this negatively impacts system cost and complexity. For proton-conducting MS-SOECs, if truly dry H_2 is maintained on the hydrogen side, many metals will avoid oxidation including Ni, Fe, and Cu, expanding the choice of metal or alloy support material. Leakage of steam or oxygen from the other side, however, would risk rapid oxidation of the support.

4. R&D opportunities and recommendations

Notably, the unique advantages of MS-SOECs have yet to be demonstrated. The impact of rapid thermal excursions, start-up/shut-down cycling, redox cycling of the cathode (e.g. by switching between steam and hydrogen), electrochemical compression, and other aggressive operating conditions on performance and durability has not been determined. It is recommended to intermittently monitor OCV when undertaking such tests, because they may result in electrolyte damage. When performing electrolysis operation, a drop in OCV due to electrolyte leakage appears as a false improvement in performance (increased current at fixed voltage, or decreased voltage at fixed current). Switching between steam-, CO_2-

, and co-electrolysis would also be interesting, as it could open up the possibility for a single stack to utilize various feed streams in an industrial plant. At this point, ASCs have better performance and degradation rate than MS-SOECs. Once other clear advantages of MS-SOECs relative to ASCs are demonstrated, applications for which these advantages are critical must be identified, to provide a clear value proposition for the MS-SOEC architecture. For example, electrolysis use cases that require rapid thermal excursions or many start-up/shut-down cycles would appear to be well-suited for MS-SOEC deployment. Integration of MS-SOECs into stacks and systems that address these applications must also be considered. Modeling is expected to facilitate cell optimization, integration into stacks, and prediction of performance under various use cases.

Oxide-conducting MS-SOECs show promise, but must be further improved. The limited long-term testing results reported so far do not allow a conclusion about the critical design, processing, or composition choices for long-term durability, but it is interesting to note that the earliest degradation reported remains the lowest (Table 1, [37]). The impact of these parameters on performance and durability needs more attention. Recent improvements in MS-SOFC design and processing should be applied to MS-SOECs. It is also imperative to seek optimal materials, structures and processing specific to MS-SOEC applications. For example, catalyst compositions and processing may need to be tuned for electrolysis operation. In several cases, use of a conventional LSCF sintered-powder anode caused low performance or delamination [42, 48], because the LSCF sintering temperature was constrained to <900°C by the presence of the metal support. This is because LSCF decomposes under the reducing sintering atmosphere required for the metal support, and the metal support would oxidize rapidly if exposed to the typical LSCF sintering temperature >1100°C in air. This underscores the importance of developing a holistic approach for fabrication of MS-SOECs that overcomes these processing limitations.

The goal of fabricating a functional proton-conducting MS-SOEC with high-conductivity electrolyte has yet to be achieved. For BZCY, deposition techniques need to be optimized for formation of a thin, dense, defect-free electrolyte layer with a suitable grain structure that enables conductivity close to that achieved for well-sintered material. The co-sintering approach can be improved by identifying sintering aids that are effective in reducing atmosphere and further developing barrier coatings on the support to suppress Si and Cr migration during sintering. SZCY should also be explored in more detail for metal-supported cells because the conductivity is almost as high as BZCY, but processing of SZCY may be more straightforward than BZCY. LCN is readily co-sintered with stainless steel, so if its conductivity can be greatly improved it may become a viable electrolyte material. Finally, other classes of proton-conducting materials should be considered for compatibility with metal supports, such as glasses and solid acids.

Oxidation of porous supports, especially in the presence of high steam content is a concern for MS-SOECs. Oxidation behavior for porous supports in steam/hydrogen with high steam content and steam/oxygen must be studied in detail. The degradation studies to date (Table 1) generally use low or moderate steam content, and the impact of high steam content must be determined in order to more fully assess the viability of the MS-SOEC design. It would be especially useful to assess degradation rate as a function of steam content. Cr evaporation from stainless steel or other Cr-containing supports should also be studied in these atmospheres. It is likely that coatings or other solutions to prevent rapid oxidation and Cr evaporation in high steam content will be needed. Optimization of support morphology to decrease internal surface area while maintaining adequate gas transport, for example by use of straight pores, deserves attention. Dry hydrogen is expected to be compatible with all metal supports, but whether breakaway oxidation occurs in this atmosphere around 600°C, especially in the presence of minor leakage, should be examined. The influence of carbon on oxidation rates of porous supports must also be addressed for co-electrolysis and other applications with carbon species.

5. Conclusions

The state of MS-SOEC development is very far behind the state of development for ASC and other conventional SOEC cell designs. The initial results indicate there is potential for the MS-SOEC design, but further work discussed in Section 4 is needed to fully assess MS-SOEC viability, especially when operated with high steam content. Continued MS-SOEC development will be useful if performance, durability, or cost can be improved beyond the other SOEC types, or if specific applications that require the unique capabilities of MS-SOEC are clearly identified. There are no fundamental limitations to the use of metal supports in SOEC conditions, but oxidation deserves attention. Oxide-conducting MS-SOECs with various electrolyte materials and fabrication approaches have been demonstrated for steam-, carbon dioxide- and co-electrolysis. Further improvement and demonstration is necessary, and it is anticipated that improvements in the adjacent MS-SOFC field will be straightforward to leverage for MS-SOEC development. For proton-conducting MS-SOECs, a processing approach that successfully overcomes the challenges associated with BZCY is yet to be developed, but early work indicates multiple paths forward.

Acknowledgements

The author thanks Ruofan Wang and Fengyu Shen for helpful discussion. This work was made possible through the HydroGEN consortium, which was funded by the U.S. Department of Energy, Office of Energy Efficiency and Renewable Energy, Fuel Cell Technologies Office under Award No. DE-EE0008079. This work was funded in part by the U.S. Department of Energy under contract no. DE-AC02-05CH11231. The views and opinions of the authors expressed herein do not necessarily state or reflect those of the United States

Government or any agency thereof. Neither the United States Government nor any agency thereof, nor any of their employees, makes any warranty, expressed or implied, or assumes any legal liability or responsibility for the accuracy, completeness, or usefulness of any information, apparatus, product, or process disclosed, or represents that its use would not infringe privately owned rights.

References

[1] Hansen JB. Solid oxide electrolysis--a key enabling technology for sustainable energy scenarios. Faraday Discuss. 2015;182:9-48.
[2] Laguna-Bercero MA. Recent advances in high temperature electrolysis using solid oxide fuel cells: A review. Journal of Power Sources. 2012;203:4-16.
[3] Pivovar B, Rustagi N, Satyapal S. Hydrogen at Scale (H2@Scale): Key to a Clean, Economic, and Sustainable Energy System. Electrochem Soc Interface. 2018;27:47-52.
[4] Zhang X, Ye L, Li H, Chen F, Xie K. Electrochemical Dehydrogenation of Ethane to Ethylene in a Solid Oxide Electrolyzer. ACS Catalysis. 2020;10:3505-13.
[5] Li W, Wang H, Shi Y, Cai N. Performance and methane production characteristics of H2O–CO2 co-electrolysis in solid oxide electrolysis cells. International Journal of Hydrogen Energy. 2013;38:11104-9.
[6] Jensen SH, Graves C, Mogensen M, Wendel C, Braun R, Hughes G, et al. Large-scale electricity storage utilizing reversible solid oxide cells combined with underground storage of CO2 and CH4. Energy & Environmental Science. 2015;8:2471-9.
[7] Martinez-Frias J. A natural gas-assisted steam electrolyzer for high-efficiency production of hydrogen. International Journal of Hydrogen Energy. 2003;28:483-90.
[8] Numata Y, Nakajima K, Takasu H, Kato Y. Carbon Dioxide Reduction on a Metal-Supported Solid Oxide Electrolysis Cell. ISIJ International. 2019;59:628-33.
[9] Hartvigsen J, Elangovan S, Elwell J, Larsen D. Oxygen Production from Mars Atmosphere Carbon Dioxide Using Solid Oxide Electrolysis. ECS Transactions. 2017;78:2953-63.
[10] Wang Y, Leung DYC, Xuan J, Wang H. A review on unitized regenerative fuel cell technologies, part B: Unitized regenerative alkaline fuel cell, solid oxide fuel cell, and microfluidic fuel cell. Renewable and Sustainable Energy Reviews. 2017;75:775-95.
[11] Gómez SY, Hotza D. Current developments in reversible solid oxide fuel cells. Renewable and Sustainable Energy Reviews. 2016;61:155-74.
[12] Lei L, Zhang J, Yuan Z, Liu J, Ni M, Chen F. Progress Report on Proton Conducting Solid Oxide Electrolysis Cells. Advanced Functional Materials. 2019;29:1903805.
[13] Dayaghi AM, Kim KJ, Kim S, Park J, Kim SJ, Park BH, et al. Stainless steel-supported solid oxide fuel cell with La 0.2 Sr 0.8 Ti 0.9 Ni 0.1 O 3−δ /yttria-stabilized zirconia composite anode. Journal of Power Sources. 2016;324:288-93.
[14] Krishnan VV. Recent developments in metal-supported solid oxide fuel cells. Wiley Interdisciplinary Reviews: Energy and Environment. 2017;6:246.

[15] Larring Y, Fontaine M-L. Critical Issues of Metal-Supported Fuel Cell. 2013:71-93.
[16] Tucker MC. Progress in metal-supported solid oxide fuel cells: A review. Journal of Power Sources. 2010;195:4570-82.
[17] Kurokawa H, Lau GY, Jacobson CP, De Jonghe LC, Visco SJ. Water-based binder system for SOFC porous steel substrates. Journal of Materials Processing Technology. 2007;182:469-76.
[18] Orera VM, Laguna-Bercero MA, Larrea A. Fabrication Methods and Performance in Fuel Cell and Steam Electrolysis Operation Modes of Small Tubular Solid Oxide Fuel Cells: A Review. Frontiers in Energy Research. 2014;2.
[19] Tucker MC. Durability of symmetric-structured metal-supported solid oxide fuel cells. Journal of Power Sources. 2017;369:6-12.
[20] Tucker MC, Ying AS. Metal-supported solid oxide fuel cells operated in direct-flame configuration. International Journal of Hydrogen Energy. 2017;42:24426-34.
[21] Tucker MC. Dynamic-temperature operation of metal-supported solid oxide fuel cells. Journal of Power Sources. 2018;395:314-7.
[22] Cho HJ, Kim KJ, Park YM, Choi GM. Flexible solid oxide fuel cells supported on thin and porous metal. International Journal of Hydrogen Energy. 2016;41:9577-84.
[23] Vasechko V, Pećanac G, Kuhn B, Malzbender J. Mechanical properties of porous ITM alloy. International Journal of Hydrogen Energy. 2016;41:562-9.
[24] Hagen A, Frandsen HL. Solid Oxide Development Status at DTU Energy. ECS Transactions. 2019;91:235-45.
[25] Santhanam S, Padinjarethil A, Tomberg M, Heddrich MP, Ansar A. Transient Operation Strategies for MW-Scale SOC Systems. ECS Transactions. 2019;91:2571-8.
[26] Zheng Y, Luo Y, Shi Y, Cai N. Dynamic Processes of Mode Switching in Reversible Solid Oxide Fuel Cells. Journal of Energy Engineering. 2017;143:04017057.
[27] Sun X, Chen M, Jensen SH, Ebbesen SD, Graves C, Mogensen M. Thermodynamic analysis of synthetic hydrocarbon fuel production in pressurized solid oxide electrolysis cells. International Journal of Hydrogen Energy. 2012;37:17101-10.
[28] Hartvigsen J, Elangovan S, Frost L. MOXIE Development Driven Prospects for ISRU and Atmosphere Revitalization. 48th International Conference on Environmental Systems. Albuquerque, New Mexico2018.
[29] Virkar AV. Mechanism of oxygen electrode delamination in solid oxide electrolyzer cells. International Journal of Hydrogen Energy. 2010;35:9527-43.
[30] Chen T, Zhou Y, Liu M, Yuan C, Ye X, Zhan Z, et al. High performance solid oxide electrolysis cell with impregnated electrodes. Electrochemistry Communications. 2015;54:23-7.
[31] Wang R, Dogdibegovic E, Lau GY, Tucker MC. Metal-Supported Solid Oxide Electrolysis Cell with Significantly Enhanced Catalysis. Energy Technology. 2019;7:1801154.
[32] Shen F, Wang R, Tucker MC. Long term durability test and post mortem for metal-supported solid oxide electrolysis cells. Journal of Power Sources. 2020;In revision.
[33] Lay-Grindler E, Laurencin J, Villanova J, Cloetens P, Bleuet P, Mansuy A, et al. Degradation study by 3D reconstruction of a nickel–yttria stabilized zirconia cathode after high temperature steam electrolysis operation. Journal of Power Sources. 2014;269:927-36.
[34] Sehested J, Gelten JAP, Helveg S. Sintering of nickel catalysts: Effects of time, atmosphere, temperature, nickel-carrier interactions, and dopants. Applied Catalysis A: General. 2006;309:237-46.
[35] Sun X, Chen M, Liu Y-L, Hjalmarsson P, Ebbesen SD, Jensen SH, et al. Durability of solid oxide electrolysis cells for syngas production. Journal of The Electrochemical Society. 2013;160:F1074-F80.
[36] Kim SJ, Choi GM. Stability of LSCF electrode with GDC interlayer in YSZ-based solid oxide electrolysis cell. Solid State Ionics. 2014;262:303-6.
[37] Schiller G, Ansar A, Lang M, Patz O. High temperature water electrolysis using metal supported solid oxide electrolyser cells (SOEC). Journal of Applied Electrochemistry. 2009;39:293-301.

[38] Hauch A, Brodersen K, Chen M, Graves C, Jensen SH, Jørgensen PS, et al. A Decade of Solid Oxide Electrolysis Improvements at DTU Energy. ECS Transactions. 2017;75:3-14.
[39] Leah RT, Bone A, Selcuk A, Rahman M, Clare A, Lankin M, et al. Latest Results and Commercialization of the Ceres Power SteelCell® Technology Platform. ECS Transactions. 2019;91:51-61.
[40] Schiller G, Ansar A, Patz O. High Temperature Water Electrolysis Using Metal Supported Solid Oxide Electrolyser Cells (SOEC). Advances in Science and Technology. 2010;72:135-43.
[41] Nechache A, Han F, Semerad R, Schiller G, Costa R. Evaluation of Performance and Degradation Profiles of a Metal Supported Solid Oxide Fuel Cell under Electrolysis Operation. ECS Transactions. 2017;78:3039-47.
[42] Han F, Nechache A, Semerad R, Costa R. Fabrication and Characterization of Metal-supported Solid Oxide Electrolysis Cells. International Conference on Electrolysis. Copenhagen, Denmark 2017.
[43] Blennow P, Hjelm J, Klemensø T, Persson As, Brodersen K, Srivastava A, et al. Development of Planar Metal Supported SOFC with Novel Cermet Anode. ECS Transactions. 2009;25:70-10.
[44] Tucker MC, Lau GY, Jacobson CP, DeJonghe LC, Visco SJ. Performance of metal-supported SOFCs with infiltrated electrodes. Journal of Power Sources. 2007;171:477-82.
[45] Dogdibegovic E, Wang R, Lau GY, Karimaghaloo A, Lee MH, Tucker MC. Progress in durability of metal-supported solid oxide fuel cells with infiltrated electrodes. Journal of Power Sources. 2019;437:226935.
[46] Wu S-H, Lin J-K, Shiu W-H, Liu C-K, Lin T-N, Lee R-Y, et al. Performance Test For Anode-Supported And Metal-Supported Solid Oxide Electrolysis Cell Under Different Current Densities. In: Salem J, editor. 42nd International Conference on Advanced Ceramics and Composites. Daytona Beach, Florida, USA: The American Ceramic Society; 2019. p. 139-48.
[47] Hwang CS, Tsai CH, Hwang TJ, Chang CL, Yang SF, Lin JK. Novel Metal Substrates for High Power Metal-supported Solid Oxide Fuel Cells. Fuel Cells. 2016;16:244-51.
[48] Lee T, Jeon S-Y, Yoo Y-S. Electrochemical Performance of a Metal-supported Solid Oxide Electrolysis Cell. KEPCO Journal on Electric Power and Energy. 2019;5:121-5.
[49] Yoo YS, Choi M, Yang S, Jin HJ, Park MA, Kim EH. Fabrication and Performance Evaluation of Solid Oxide Electrolysis Cell Integrated with Metal Interconnect by Joining Process. ECS Transactions. 2015;68:3475-80.
[50] Wang S, Inoishi A, Hong J-e, Ju Y-w, Hagiwara H, Ida S, et al. Ni–Fe bimetallic cathodes for intermediate temperature CO2 electrolyzers using a La0.9Sr0.1Ga0.8Mg0.2O3 electrolyte. Journal of Materials Chemistry A. 2013;1:12455.
[51] Wang S, Tsuruta H, Asanuma M, Ishihara T. Ni-Fe-La(Sr)Fe(Mn)O3as a New Active Cermet Cathode for Intermediate-Temperature CO2Electrolysis Using a LaGaO3-Based Electrolyte. Advanced Energy Materials. 2015;5:1401003.
[52] Ishihara T, Kusaba H, Kim HH, Kang BS. Preparation of La_{0.9}Sr_{0.1}Ga_{0.8}Mg_{0.2}O₃ Film by Pulse Laser Deposition (PLD) Method on Porous Ni–Fe Metal Substrate for CO₂ Electrolysis. ISIJ International. 2019;59:613-8.
[53] Lefebvre-Joud F, Gauthier G, Mougin J. Current status of proton-conducting solid oxide fuel cells development. Journal of Applied Electrochemistry. 2009;39:535-43.
[54] Aoki Y, Jeong S, Zhu C, Habazaki H. Origins of High Power Outputs in Hydrogen Permeable Metal-Support Fuel Cells. ECS Transactions. 2019;91:917-20.
[55] Kariya T, Tanaka H, Hirono T, Kuse T, Yanagimoto K, Uchiyama K, et al. Development of a novel cell structure for low-temperature SOFC using porous stainless steel support combined with hydrogen permeable Pd layer and thin film proton conductor. Journal of Alloys and Compounds. 2016;654:171-5.
[56] Stange M, Stefan E, Denonville C, Larring Y, Rørvik PM, Haugsrud R. Development of novel metal-supported proton ceramic electrolyser cell with thin film BZY15–Ni electrode and BZY15 electrolyte. International Journal of Hydrogen Energy. 2017;42:13454-62.

[57] Stefan E, Stange M, Denonville C, Larring Y, Hildenbrand N, Norby T, et al. Layered microstructures based on BaZr0.85Y0.15O3−δ by pulsed laser deposition for metal-supported proton ceramic electrolyser cells. Journal of Materials Science. 2017;52:6486-97.
[58] Han F, Zhou X, Dayaghi AM, Norby T, Stange M, Sata N, et al. Development of Metal Supported Cells Using BaZrO3-Based Proton Conducting Ceramics. ECS Transactions. 2019;91:1035-45.
[59] Stange M, Dayaghi AM, Denonville C, Larring Y, Rørvik PM, Haugsrud R, et al. Fabrication of Metal-Supported Proton-Conducting Electrolysers with Thin Film Sr- and Ce-Doped BZY Electrolyte. ECS Transactions. 2019;91:941-9.
[60] Yamazaki Y, Hernandez-Sanchez R, Haile SM. High Total Proton Conductivity in Large-Grained Yttrium-Doped Barium Zirconate. Chemistry of Materials. 2009;21:2755-62.
[61] Zhu T. Thin-Film, Metal-Supported High-Performance and Durable Proton-Solid Oxide Electrolyzer Cell. Hydrogen and Fuel Cells Program Annual Merit Review. Crystal City, Virginia2019.
[62] Myles TD, Ouimet R, Kwak D, Maric R. Characterization and Performance of Proton Conducting Solid Oxide Fuel Cells Manufactured Using Reactive Spray Deposition Technology. ECS Transactions. 2016;72:17-23.
[63] Wang R, Byrne C, Tucker MC. Assessment of co-sintering as a fabrication approach for metal-supported proton-conducting solid oxide cells. Solid State Ionics. 2019;332:25-33.
[64] Wang R, Lau GY, Ding D, Zhu T, Tucker MC. Approaches for co-sintering metal-supported proton-conducting solid oxide cells with Ba(Zr,Ce,Y,Yb)O3-δ electrolyte. International Journal of Hydrogen Energy. 2019;44:13768-76.
[65] Vafaeenezhad S, Sandhu NK, Hanifi AR, Etsell TH, Sarkar P. Development of proton conducting fuel cells using nickel metal support. Journal of Power Sources. 2019;435:226763.
[66] Henry S, Galerie A, Antoni L. Abnormal Oxidation of Stabilized Ferritic Stainless Steels in Water Vapor. Materials Science Forum. 2001;369-372:353-60.
[67] Yuan J, Wu X, Wang W, Zhu S, Wang F. Investigation on the Enhanced Oxidation of Ferritic/Martensitic Steel P92 in Pure Steam. Materials (Basel). 2014;7:2772-83.
[68] Stange M, Denonville C, Larring Y, Brevet A, Montani A, Sicardy O, et al. Improvement of corrosion properties of porous alloy supports for solid oxide fuel cells. International Journal of Hydrogen Energy. 2017;42:12485-95.
[69] Karczewski J, Brylewski T, Miruszewski T, Andersen KB, Jasinski PZ, Molin S. High-temperature kinetics study of 430L steel powder oxidized in air at 600–850 °C. Corrosion Science. 2019;149:100-7.
[70] Molin S, Gazda M, Jasinski P. Coatings for improvement of high temperature corrosion resistance of porous alloys. Journal of the European Ceramic Society. 2011;31:2707-10.
[71] Molin S, Gazda M, Jasinski P. High temperature oxidation of porous alloys for solid oxide fuel cell applications. Solid State Ionics. 2010;181:1214-20.
[72] Reiss G, Frandsen HL, Persson ÅH, Weiß C, Brandstätter W. Numerical evaluation of oxide growth in metallic support microstructures of Solid Oxide Fuel Cells and its influence on mass transport. Journal of Power Sources. 2015;297:388-99.
[73] Palcut M, Mikkelsen L, Neufeld K, Chen M, Knibbe R, Hendriksen PV. Corrosion stability of ferritic stainless steels for solid oxide electrolyser cell interconnects. Corrosion Science. 2010;52:3309-20.
[74] Alnegren P, Sattari M, Froitzheim J, Svensson JE. Degradation of ferritic stainless steels under conditions used for solid oxide fuel cells and electrolyzers at varying oxygen pressures. Corrosion Science. 2016;110:200-12.
[75] Stefan E, Neagu D, Blennow Tullmar P, Persson ÅH, Sudireddy BR, Miller D, et al. Spinel-based coatings for metal supported solid oxide fuel cells. Materials Research Bulletin. 2017;89:232-44.
[76] Stefan E, Denonville C, Larring Y, Stange M, Haugsrud R. Oxidation study of porous metal substrates for metal supported proton ceramic electrolyzer cells. Corrosion Science. 2020;164:108335.

[77] Skilbred AWB, Haugsrud R. Sandvik Sanergy HT – A potential interconnect material for LaNbO4-based proton ceramic fuel cells. Journal of Power Sources. 2012;206:70-6.
[78] Wang R, Sun Z, Choi J-P, Basu SN, Stevenson JW, Tucker MC. Ferritic stainless steel interconnects for protonic ceramic electrochemical cell stacks: Oxidation behavior and protective coatings. International Journal of Hydrogen Energy. 2019;44:25297-309.
[79] Cheng X, Jiang Z, Monaghan BJ, Wei D, Longbottom RJ, Zhao J, et al. Breakaway oxidation behaviour of ferritic stainless steels at 1150°C in humid air. Corrosion Science. 2016;108:11-22.
[80] Alnegren P, Sattari M, Svensson J-E, Froitzheim J. Temperature dependence of corrosion of ferritic stainless steel in dual atmosphere at 600–800 °C. Journal of Power Sources. 2018;392:129-38.
[81] Reisert M, Berova V, Aphale A, Singh P, Tucker MC. Oxidation of Porous Stainless Steel Supports for Metal-Supported Solid Oxide Fuel Cells. International Journal of Hydrogen Energy. 2020;In review.
[82] Xu N, Chen M, Han M. Oxidation behavior of a Ni-Fe support in SOFC anode atmosphere. Journal of Alloys and Compounds. 2018;765:757-63.